



## Research paper

# Highly-efficient photocatalytic disinfection of *Escherichia coli* under visible light using carbon supported Vanadium Tetrasulfide nanocomposites

Baogang Zhang<sup>a,1,\*</sup>, Shiqiang Zou<sup>b,1</sup>, Ruquan Cai<sup>a</sup>, Min Li<sup>a</sup>, Zhen He<sup>b,\*</sup>

<sup>a</sup> School of Water Resources and Environment, MOE Key Laboratory of Groundwater Circulation and Environmental Evolution, China University of Geosciences (Beijing), Beijing 100083, China

<sup>b</sup> Department of Civil and Environmental Engineering, Virginia Polytechnic Institute and State University, Blacksburg, VA 24061, USA



## ARTICLE INFO

**Keywords:**  
Vanadium Tetrasulfide  
Photocatalytic disinfection  
*Escherichia coli*  
Nanocomposites  
Visible light

## ABSTRACT

Reliable and effective water disinfectants are of paramount importance to address mounting health concerns in drinking water. Herein, Vanadium Tetrasulfide (VS<sub>4</sub>) nanocomposites supported by different carbon materials, including VS<sub>4</sub>/CP (carbon powder), VS<sub>4</sub>/rGO (reduced graphene oxides), VS<sub>4</sub>/CF (carbon fiber), and VS<sub>4</sub>/CNT (carbon nanotube), were synthesized, comprehensively characterized, and investigated as photocatalytic disinfectants. Among them, the cost-effective and lattice-structure VS<sub>4</sub>/CP exhibited the best disinfection performance for removing *E. coli* (Gram-negative) under both simulated visible light and sunlight, with a maximum inactivation rate of 9.7 log at 0.1 g L<sup>-1</sup> in 30 min. However, it was not very effective to eliminate *S. aureus* (Gram-positive bacteria) with a disinfection rate of 1.7 log inactivation in 30 min. Consistent disinfection performance was confirmed with four successive stability tests and over a wide range of *E. coli* density (6 log to 9 log CFU ml<sup>-1</sup>). The potential disinfection mechanism was studied on a subcellular level, indicating that membrane damage (via mineralization, lipid peroxidation and collapsed membrane potential) and penetration-induced intracellular damage including DNA degradation and decreased ATP level could be the main inactivation principles. Further photochemical investigation suggested that ·O<sub>2</sub><sup>-</sup>, h<sup>+</sup> and e<sup>-</sup> were crucial active species, and an acidic/neutral environment would favor the photocatalytic disinfection. These results have demonstrated effectiveness and potential applications of the developed VS<sub>4</sub>/CP nanocomposites in water disinfection.

## 1. Introduction

Efficient water disinfection methods are urgently required to sustainably address drinking water safety issues [1]. Current disinfection approaches, i.e. externally added chemical reagents, excel in eliminating a majority of pathogens in both drinking water treatment plants and subsequent distribution systems [2], thereby significantly reducing outbreaks of waterborne disease. However, the disinfection byproducts (DBPs) originated from chlorine and chlorine-based chemical disinfectants create potential health concerns as DBPs are considered to be carcinogens, mutagens, and teratogens [3]. The alternative ozone and UV inactivation are much safer but more energy-intensive, rendering elevated operational cost. Hence, DBP-free energy-efficient disinfectants are of strong interest to address drinking water challenges. Recently, nanomaterials (NMs) with photocatalytic properties, such as titanium dioxide (TiO<sub>2</sub>) and its derivatives [4], magnesium oxide (MgO) [5], calcium oxide (CaO) [6,7], zinc oxide (ZnO) [8], and aluminum oxide (Al<sub>2</sub>O<sub>3</sub>) [9], have been extensively investigated as next

generation disinfectants. Compared to conventional disinfectants, e.g. ozone and UV inactivation, photocatalytic NMs offer broader applications in drinking water treatment, for example simultaneous decolorization and advanced oxidation of persistent organic pollutants (POPs), serving as cost-effective (commercially available), easy-to-use (direct addition with no pretreatment), and chemically stable (long-term stability for continuous application) multipurpose disinfectants. Separation of photocatalytic NMs can be easily achieved via membrane separation to render high-quality product water [10,11]. However, most metal oxide NMs (e.g. TiO<sub>2</sub>) need to be activated under UV light (typically UVA and UVB, ~4% energy of solar spectrum [12]) while exhibiting a poor disinfection rate under visible light exposure due to a large band gap (e.g. 3.0–3.2 eV, TiO<sub>2</sub> [13]). To lower the band gaps for visible light activation, metal doping, especially with noble metals, has been performed to facilitate energy harness of visible-range photons and enhance visible light absorbance [14]. Yet the doping expense and complicated preparation procedures impede practical application and extensive use.

\* Corresponding authors.

E-mail addresses: [baogangzhang@cugb.edu.cn](mailto:baogangzhang@cugb.edu.cn) (B. Zhang), [zhenhe@vt.edu](mailto:zhenhe@vt.edu) (Z. He).

<sup>1</sup> These authors contributed equally to this work.

Lacking fundamental understanding of disinfection mechanisms, especially at a subcellular level, is considered to be another impedance towards comprehensive applications of photocatalytic NMs in drinking water treatment [15]. Efficient inactivation of bacteria often involves interruption or complete destruction of their essential physiological functions, including cell membrane, cytoplasm, and nucleic acids [16]. Malfunctions of cell membrane can be induced by changes of membrane permeability [17], degeneration of attached protein [18], lipid peroxidation [19], and disorder of membrane potential [20]. Within cell cytoplasm, interruption of the synthesis of core enzymes and protein degradation are acknowledged to render failure of self-repair and eventually bacteria inactivation [18]. Irreversible damage to bacteria nucleic acids, e.g. through UV exposure, will lead to rapid cell death [21]. Nonetheless, previous studies have observed bacterial inactivation via NMs under dark environment [15], encouraging comprehensive investigation for better understanding of subcellular disinfection mechanisms.

In our previous study, Vanadium Tetrasulfide ( $\text{VS}_4$ )/carbon powder ( $\text{VS}_4/\text{CP}$ ) nanocomposites were proposed as a photocatalyst for excellent decolorization performance [22].  $\text{VS}_4$  is a metal chalcogenide that has received limited attention in the past [23], with a primary focus on an energy storage material within the lithium battery system due to its high charge capacity [24]. The visible-light-driven photocatalytic property of  $\text{VS}_4$  was confirmed in water splitting experiment with desirable hydrogen gas generation [25], resulting from efficient generation of highly oxidative radicals that could be potentially applied to disinfection. Further doping with different forms of carbon, including carbon powder (CP), reduced graphene oxide (rGO), carbon fiber (CF), and carbon nanotube (CNT), not only supposed to increase the visible light absorbance of photocatalysts (e.g.  $\text{TiO}_2$ ) with enhanced photo-excitation [26,27], but may also promote intra-aggregation with mesoporous structure and potentially higher efficiency [28,29]. The specific objectives of this study were to (1) characterize various carbon supported  $\text{VS}_4$  nanocomposites and evaluate their photocatalytic disinfection performance; (2) examine the disinfection performance of  $\text{VS}_4/\text{CP}$  nanocomposites under different light conditions as well as disinfection stability by using *Escherichia coli* (*E. coli*) as indicators; (3) systematically analyze the key factors that could affect the photocatalytic disinfection of  $\text{VS}_4/\text{CP}$  towards optimized inactivation rate, such as pH, catalyst dosage, *E. coli* concentration and irradiation condition; (4) investigate the disinfection mechanism on a subcellular level via systematic analysis of cell morphology, potassium ion ( $\text{K}^+$ ) leakage, total organic carbon (TOC) concentration, cell membrane permeability, lipid peroxidation, membrane potential, membrane protein, intracellular enzyme degradation, cellular ATP level, and DNA fragment analysis; and (5) explore the disinfection mechanism on a photo-chemistry level via a scavenger study focusing on generated active species.

## 2. Methods and materials

### 2.1. Synthesis of carbon supported $\text{VS}_4$ nanocomposites

A simple one-step hydrothermal synthesis method was performed to obtain the  $\text{VS}_4/\text{CP}$  nanocomposite according to a previous study [22]. Briefly, 0.448 g of CP was uniformly dispersed in 30 mL deionized (DI) water using ultrasonic oscillation (~0.5 h) to form a homogenous solution. Sodium orthovanadate (0.9 g) and thioacetamide (2.5 g) were gradually added to the above solution during continuous stirring (30 min). The obtained solution was transferred to a 50-mL Teflon-lined stainless steel autoclave and maintained at 150 °C for 12 h. Once the autoclave was sufficiently cooled down to room temperature, the nanocomposite products were centrifuged at 4000 rpm, and washed with DI water and ethyl alcohol for several times before being dried in a vacuum drying oven at 60 °C (6 h). The blank control of  $\text{VS}_x$  was prepared by using the same method with no CP addition. Synthesis of  $\text{VS}_4/$

rGO,  $\text{VS}_4/\text{CF}$ , and  $\text{VS}_4/\text{CNT}$  were following a previous study [24]. The final nanocomposite product contained 5 wt% carbon theoretically (an optimized condition [24]).

### 2.2. Characterization of synthesized nanocomposites

The synthesized nanocomposites were analyzed by energy dispersive X-ray (EDX) on a JEOL JAX-840 scanning electron microscope (SEM) operated at 20 kV (JEOL JAX-840, Hitachi Limited, Japan). X-ray diffraction (XRD) measurement was performed with a Cu-K $\alpha$  ( $\lambda = 1.5405 \text{ \AA}$ ) as a radiation source operated at 40 kV and 200 mA (Rigaku-D/MAX-PC 2500, Rigaku, Japan). The XRD pattern was analyzed by using Jade 6 software. The transmission electron microscope (TEM) images were obtained on a JEOL TEM system operated at 200 kV (JEM-2100, Hitachi Limited, Japan). X-ray photoelectron spectroscopy (XPS) measurements were carried out using a Kratos XSAM-800 spectrometer (UK) with an Mg-K $\alpha$  radiator.

### 2.3. Photocatalytic disinfection experiment

The photocatalytic disinfection performance of various carbon supported  $\text{VS}_4$  nanocomposites was examined by the bacteria inactivation rate of *E. coli* as an indicator. *E. coli* strain was purchased directly from American Type Culture Collection (ATCC 15597), cultivated with Luria-Bertani medium (200 rpm), and harvested via centrifuge at 6000 rpm (6 min and 4 °C). For every batch test, a specific amount of carbon supported  $\text{VS}_4$  nanocomposites were added to a double-layer beaker (100 mL inside volume, sterilized) filled with DI water to form a 50-mL homogenous solution (with ultrasonic oscillation). The *E. coli* solution (a specific volume,  $5 \times 10^9$  colony forming unit (CFU) mL $^{-1}$ ) was then added to provide a determined initial *E. coli* concentration, followed by continuous magnetic stirring throughout the test. The default disinfection system had a carbon supported  $\text{VS}_4$  dosage of 0.1 g L $^{-1}$ , a solution pH of 7, and an initial *E. coli* density of  $10^9$  CFU mL $^{-1}$ , exposed under simulated visible light (300 W CEL-HXF300E xenon lamp, CEAULIGHT, China) with a 420 nm cut-off filter. Circulating cooling water bath was employed to accelerate heat dispersion (generated by the light) towards a stable system temperature (25 °C). In addition to *E. coli* (Gram-negative), *S. aureus* (ATCC 25923, Gram-positive) suspension was also prepared by the same cultivation approach with a comparable initial concentration of  $10^9$  CFU mL $^{-1}$ . Each batch test lasted for 30 min with samples (0.5 mL) taken at a 6-min interval. All collected samples were resuspended in DI water (4.5 mL) with 0.1 mL transferred to coated plate (triplicate) and cultured under 37 °C for 24 h before cell counting (with a limit of detection of 10 CFU mL $^{-1}$  and a limit of quantification of 200–300 CFU mL $^{-1}$ , respectively).

The comparison of disinfection performance among  $\text{VS}_x$  (blank control),  $\text{VS}_4/\text{CP}$ ,  $\text{VS}_4/\text{rGO}$ ,  $\text{VS}_4/\text{CF}$ , and  $\text{VS}_4/\text{CNT}$  was performed in the default disinfection system with the same dosage of 0.1 g L $^{-1}$ . Due to its desirable performance and cost-effective feature, the  $\text{VS}_4/\text{CP}$  nanocomposites were further evaluated under different light conditions, including dark environment, simulated visible light (100 W m $^{-2}$ , referred as visible light unless otherwise stated, lamp experiment), and natural sunlight (outdoor experiment). The natural sunlight was directly obtained with sunshine between 10 a.m. and 4 p.m. of a day (~379.2 W m $^{-2}$  [30]). The stability of  $\text{VS}_4/\text{CP}$  as disinfectant was investigated under visible light successively for four 30-min cycles. After each cycle, the  $\text{VS}_4/\text{CP}$  nanocomposites were separated from liquid phase via filtration (0.22  $\mu\text{m}$  filter paper) and reapplied in next cycle without further regeneration. The key factors that could affect the disinfection performance were systematically investigated, including initial solution pH (4, 5, 6, 7, 8, and 9), catalyst dosage (0.05 g L $^{-1}$ , 0.1 g L $^{-1}$ , 0.2 g L $^{-1}$ , and 0.4 g L $^{-1}$ ), and initial *E. coli* density ( $10^6$  CFU mL $^{-1}$ ,  $10^7$  CFU mL $^{-1}$ ,  $10^8$  CFU mL $^{-1}$ , and  $10^9$  CFU mL $^{-1}$ ).

#### 2.4. Disinfection mechanism study

The possible disinfection mechanism of VS<sub>4</sub>/CP in the default disinfection system was first studied on a subcellular level via a systematic analysis of cell morphology, total organic carbon (TOC), potassium ion (K<sup>+</sup>) leakage, cell membrane permeability, lipid peroxidation, membrane potential, intracellular enzyme degradation, cellular ATP level, and DNA amount. Detailed methods were based on previous studies [16,31]. In brief, for *E. coli* cell morphology analysis, 10 mL suspension was sampled from the disinfection system, followed by vacuum filtration through the 0.22 μm Millipore membrane. The *E. coli* cells obtained on the membrane were resuspended in sterilized ultrapure water, fixed on copper grids, and then observed via TEM and environmental scanning electron microscope (ESEM, Quanta 200 FEG, FEI, USA). The TOC and potassium ion (K<sup>+</sup>) levels in the filtered samples were quantified at a 6-min interval via TOC-V<sub>CPN</sub> (Shimadzu, Kyoto, Japan) and flame atomic absorption spectrophotometer (Analytik Jena, Germany), respectively. The corresponding maximum K<sup>+</sup> level was quantified from the lysed cells after ultrasonication [16]. Cell membrane integrity was evaluated with respect to membrane permeability quantified by penetration of extracellular substrate (o-nitrophenyl-β-D-galactopyranoside, ONPG) into cytoplasm and lipid peroxidation via measuring the peroxidation product malondialdehyde (MDA), and membrane potential [19] according to Long et al. [16]. Cytoplasmic components including cellular ATP level, intracellular enzyme degradation, and DNA extraction were determined commercial kits referring to previous study [16]. PCR was performed using universal primers, F27 (5'-AGAGTTTGAT-CMTGGCTCAG-3') and reverse primer R1492 (5'-TTGGYTACCTTGTT-ACGACT-3') [32]. Nearly full length 16S rRNA gene (~1500 bp), instead of a specific target gene, was amplified [33]. PCR products were visualized by electrophoresis in a 0.8% agarose gel at 130 V for 25 min, and stained with the Gelred dye.

#### 2.5. Functional scavenger study

To better understand the disinfection mechanism of VS<sub>4</sub>/CP on a photochemistry level, functional scavenger compounds were added to the default disinfection system to remove the corresponding active species under visible light irradiation [6]: Fe(II)-EDTA (0.1 mM) for H<sub>2</sub>O<sub>2</sub> removal, sodium oxalate (Na<sub>2</sub>C<sub>2</sub>O<sub>4</sub>, 0.05 mM) for h<sup>+</sup> elimination, Cr(VI) (5 mM) for e<sup>-</sup> scavenging, isopropanol for ·OH removal, and 4-hydroxy-2,2,6,6-tetramethyl-piperidinyloxy (TEMPO, 2 mM) to neutralize ·O<sub>2</sub><sup>-</sup>. The concentrations listed above were the optimized conditions according to a previous study [34]. Scavenger study without VS<sub>4</sub>/CP addition was also performed to rule out the potential disinfection effect of scavenger compounds. Samples were taken at a 6-min interval for 30 min, filtrated by 0.22 μm millipore membrane to remove the VS<sub>4</sub>/CP nanocomposites particles, and tested for disinfection performance via cell density quantification.

### 3. Results and discussion

#### 3.1. Characterization of carbon supported VS<sub>4</sub> nanocomposites

The structures and element compositions of the prepared carbon supported VS<sub>4</sub> nanocomposites were first investigated via multiple characterization techniques. For all carbon supported nanocomposites, uniformly distributed nanoparticles were observed on the carbon matrix with a size of 50–100 nm as shown in TEM images (Fig. 1 A-D), whereas VS<sub>x</sub> (blank control) exhibited a thin film structure (no lattice observed, Fig. 1E). It should be noted that a clear lattice structure was observed in VS<sub>4</sub>/CP with a lattice spacing of ~0.56 nm (Fig. 1F), which was also reported by a previous study of VS<sub>4</sub> nanostructure [24]. Further elemental mapping (Fig. A1, in Supplementary material) revealed higher element counts of vanadium (V, green color) and sulfur (S, yellow) on the black background, combined with elemental carbon (C,

red). The stoichiometric mole ratio of S to V was determined to be 22:5.4 (or 4.07:1) via color intensity on mapping, close to a theoretical ratio of 4 in VS<sub>4</sub>. The major peaks detected via SEM-EDX in VS<sub>4</sub>/CP, VS<sub>4</sub>/rGO, VS<sub>4</sub>/CF, and VS<sub>4</sub>/CNT also confirmed an element composition of C, V and S within the material (S/V ratio of 4, Fig. 2A). However, VS<sub>x</sub> exhibited a notable higher V peak, indicating a different composition than VS<sub>4</sub>. The XRD pattern revealed the nanostructure with a diffraction peak corresponding to the (110) plane at 15.8° ([JCPDS No. 072-1294], Fig. 2B), indicating a monoclinic phase of nanoparticles [35]. Other peaks, such as carbon at 16.7° and sulfur at 22.8°, were assigned to the (020) and (101) diffraction ([JCPDS No. 024-1206]), respectively [24]. XPS was employed to probe the electronic structures inside various nanocomposites (Fig. 3A). The C 1s peak located at 284.4 eV suggested the C–C bond, while the fitted peak at 287.8 eV revealed a trace amount of oxygen-containing functional groups (Fig. 3B), considering that the majority of those groups were effectively eliminated via the hydrothermal process [24]. The S 2p core level analysis confirmed the existence of the S<sub>2</sub><sup>2-</sup> species [25], and the peaks at 162.3 and 163.5 eV can be indexed to S 2p<sub>3/2</sub> and S 2p<sub>1/2</sub> within S<sub>2</sub><sup>2-</sup> dimer, respectively (Fig. 3C). Comparing to VS<sub>x</sub>, shifting to a lower binding energy was observed and should credit to the formation of C-S bond and potential chemical interaction between VS<sub>4</sub> and carbon material (Fig. 3D). The V 2p peaks located at 513.7 and 517.1 eV could be ascribed to binding energies of V 2p<sub>3/2</sub> and V 2p<sub>1/2</sub> (Fig. 3D), confirming the existence of V<sup>4+</sup>. These results have demonstrated successful formation of V<sup>4+</sup> and (S<sub>2</sub><sup>2-</sup>)<sub>2</sub> within the carbon supported nanocomposites, compared to that of VS<sub>x</sub>.

#### 3.2. Disinfection performance and stability of carbon supported VS<sub>4</sub> nanocomposites

Photocatalytic disinfection capability of VS<sub>4</sub>/CP, VS<sub>4</sub>/rGO, VS<sub>4</sub>/CF, VS<sub>4</sub>/CNT and VS<sub>x</sub> was evaluated in the default disinfection system with the same dosage of 0.1 g L<sup>-1</sup>. The *E. coli* density in the VS<sub>x</sub> system was rather stable, indicating a failure of photocatalytic inactivation (Fig. 4A). On the other hand, gradual decrease of *E. coli* density was observed in all four carbon supported VS<sub>4</sub> systems. Among them, VS<sub>4</sub>/CP and VS<sub>4</sub>/rGO had the most desirable disinfection rate with *E. coli* below detection limit at the end of experiment. Hence, carbon materials was demonstrated to greatly enhance photocatalytic disinfection performance [26,27].

Considering the cost of rGO, the more cost-effective VS<sub>4</sub>/CP nanocomposite was further investigated for disinfection performance under different light conditions, including dark environment, visible light (lamp experiment), and natural sunlight (outdoor experiment). An experiment system without VS<sub>4</sub>/CP was placed under visible light serving as a blank control, and *E. coli* density was constant throughout the 30-min test (black line, Fig. 4B). Likewise, VS<sub>4</sub>/CP under dark environment did not achieve obvious inactivation of *E. coli*, indicating the importance of light exposure to disinfection. When a light source was provided, either visible light or natural sunlight, a near linear decrease of *E. coli* density from ~10<sup>8</sup> CFU mL<sup>-1</sup> to 0 within 30 min (blue and cyan lines) was obtained. This comparable inactivation rates exposed under sunlight and simulated visible light has been confirmed in other photodisinfection studies [36], and the performance was much more efficient than direct solar water disinfection (SODIS, 6–48 h) proposed by World Health Organization [37]. It should be noted that natural sunlight could lead to an overall retardation of disinfection process, and hence a much higher irradiance value (~379.2 mW m<sup>-2</sup>) would be required to render comparable disinfection performance with that of simulated visible light (100 mW m<sup>-2</sup>). The results confirmed efficient photocatalytic disinfection capability of VS<sub>4</sub>/CP nanocomposites under illumination, and sunlight-driven disinfection could further reduce operation cost in future applications. The VS<sub>4</sub>/CP required much less disinfection time (only 0.5 h) compared to similar visible-light-driven nanomaterial disinfectants (1.0–4.0 h, Table 1). The obtained

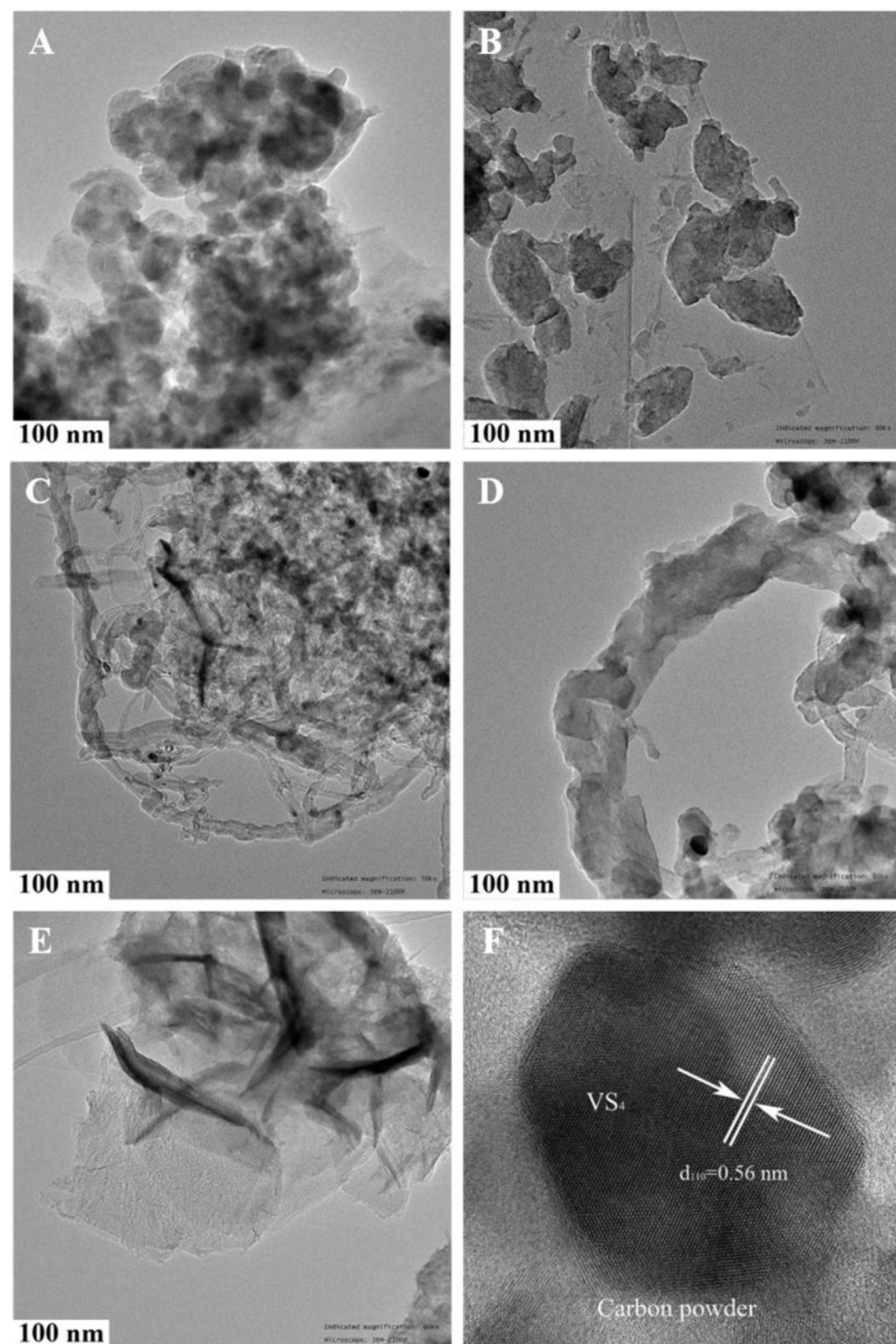


**Fig. 1.** TEM images of different carbon supported VS<sub>4</sub> nanocomposites: (A) VS<sub>4</sub>/CP, (B) VS<sub>4</sub>/rGO, (C) VS<sub>4</sub>/CF, (D) VS<sub>4</sub>/CNT, (E) VS<sub>x</sub> (no carbon support material), and (F) VS<sub>4</sub>/CP lattice.

inactivation rate (7.7 log at 0.01 g L<sup>-1</sup>) was also superior than that treating comparable *E. coli* density (10<sup>6</sup>–10<sup>7</sup> CFU mL<sup>-1</sup>) under similar photodisinfect dosage (0.02–0.20 g L<sup>-1</sup>), ranging from 3.0 log to 7.0 log (Table 1) [38–43]. It is worth noting that the proposed VS<sub>4</sub>/CP was less effective to inactivate *S. aureus* (Gram-positive bacteria), exhibiting a normalized disinfection rate of 1.7 log inactivation of *S. aureus* in 30 min. The difference of deactivating rate between Gram-positive and Gram-negative bacteria might be attributed to their cell wall structure. Gram-positive bacteria usually have a thicker cell wall composed of many layers of peptidoglycan and teichoic acids, presenting a natural barrier to disinfectants. Gram-negative bacteria, though possessing an extra outer membrane, have a thinner cell wall and hence more

sensitive to VS<sub>4</sub>/CP nanocomposites [44]. Future study could focus on higher VS<sub>4</sub>/CP dosage or extended disinfection time to enhance inactivation rate of Gram-positive bacteria (not studied here) and further boost its competitiveness over conventional disinfection methods (e.g. UV/H<sub>2</sub>O<sub>2</sub>).

Subsequent stability test (under visible light) revealed the excellent disinfection performance of VS<sub>4</sub>/CP nanocomposites even after four-time applications. All *E. coli* cells were eliminated within 30 min with comparable *E. coli* density profiles (below detection limit, Fig. 4C). Compared to conventional chemical-based disinfectants, the VS<sub>4</sub>/CP nanocomposites exhibited a stable disinfection performance over an extended period of time and possessed a potential for practical

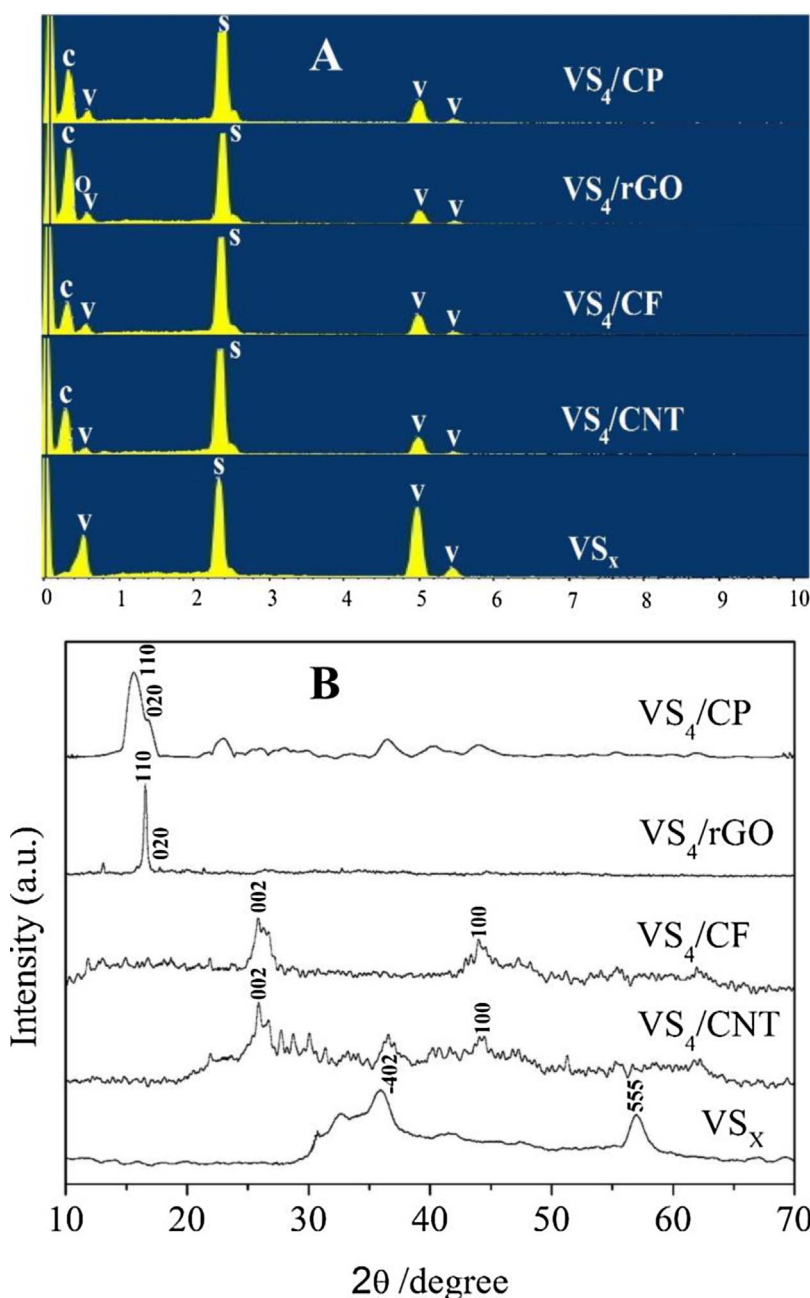


**Fig. 2.** Characterization of different carbon supported VS<sub>4</sub> nanocomposites regarding (A) EDX and (B) XRD.

application. It should be noted that no regeneration process was required after each test, suggesting a well-lasting lifespan of VS<sub>4</sub>/CP that may result in a low operational cost. Leaching of toxic Vanadium was confirmed to be negligible in aqueous solution (less than 1% of the vanadium mass loading) [22].

### 3.3. Factors influencing photocatalytic disinfection by VS<sub>4</sub>/CP

The key factors that could affect the photocatalytic disinfection performance were systematically investigated towards an optimized inactivation rate. The initial solution pH was adjusted to 4, 5, 6, 7, 8, and 9, and enhanced inactivation efficiency was observed under an acidic environment (Fig. 5A). When an initial pH was decreased from 8 to 7, all *E. coli* cells could be eliminated within 30 min (below detection limit). Further decrease of the initial pH to 4 resulted in elimination of bacteria (100%) in just 24 min and the highest inactivation rate of 7.7 log. It should be noted that, if no VS<sub>4</sub>/CP was added, relatively stable *E.*

*coli* concentration was observed in 30 min within a pH range of 4–9, and an inhibitory effect could only be observed with a pH below 4 (Fig. A2) [45]. Photocatalytic disinfection via VS<sub>4</sub>/CP nanocomposites is likely due to generation of active species, such as  $\text{s}\cdot\text{OH}$ ,  $\text{H}_2\text{O}_2$ ,  $\cdot\text{O}_2^-$ ,  $e^-$ , and  $\text{h}^+$  generated by through Eqs. (1) – (4) [46]. Clearly, solution pH is a key factor as a high concentration of  $\text{H}^+$  would facilitate the generation of active species according to Eqs. (2), (3) and (4). A basic environment would impede bacteria cell inactivation, rendering an undesirable 1.1 log inactivation of *E. coli* even after 30 min. Based on the obtained results, the VS<sub>4</sub>/CP nanocomposites exhibited excellent inactivation performance under both acidic and neutral environment, suggesting a potential applicability for disinfection of water or treated wastewater (pH = 7.3 [47]).



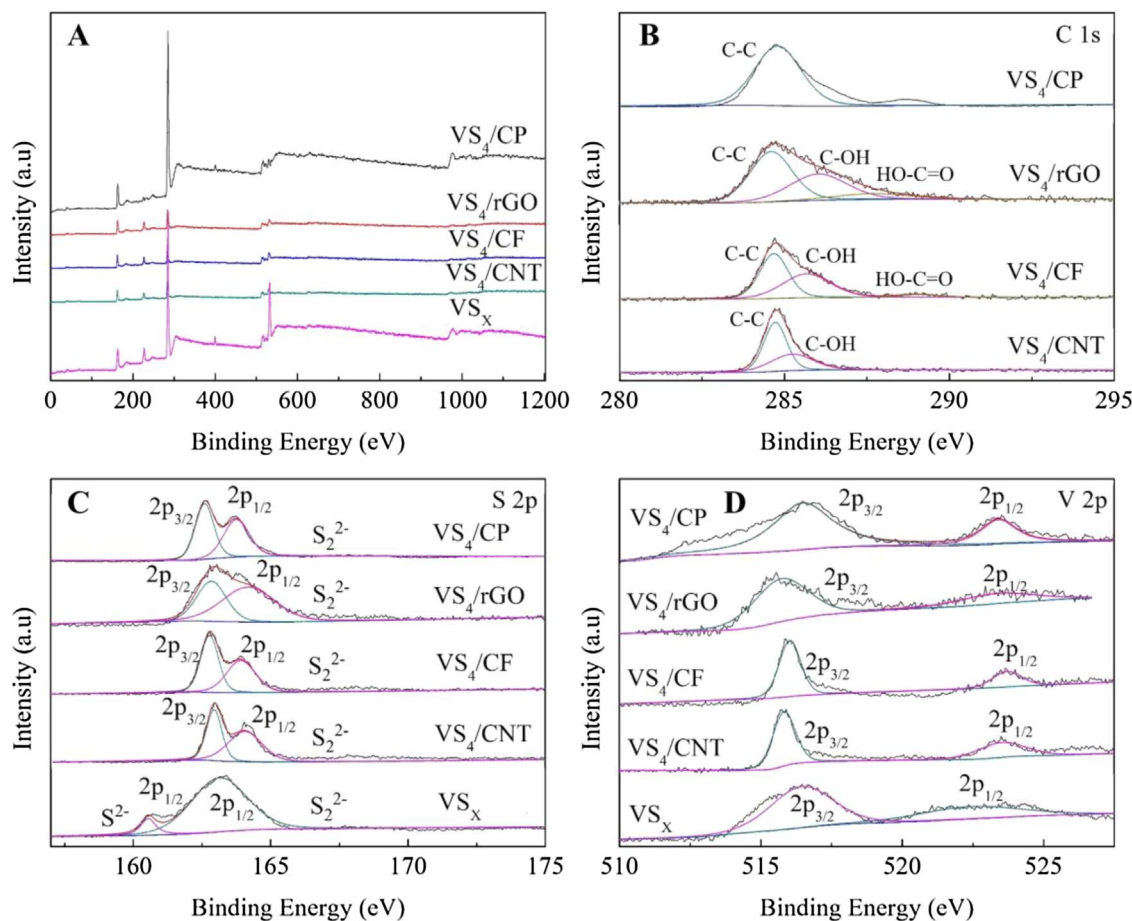
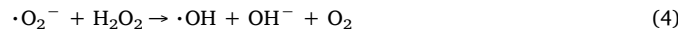


Fig. 3. XPS characterization of different carbon supported  $\text{VS}_4$  nanocomposites regarding (A) survey spectrum, (B) C 1s, (C) S 2p, and (D) V 2p.



Disinfectant dosage is another key factor for disinfection efficiency that should be investigated (Fig. 5B). With the increase of dosage, more photons could be absorbed by  $\text{VS}_4/\text{CP}$  (acting as active centers), and hence the inactivation rate was increased from 5.6 log at 0.05 g L<sup>-1</sup> in 30 min to 7.7 log at 0.2 g L<sup>-1</sup> in 24 min. However, further dosage increase from 0.2 g L<sup>-1</sup> to 0.4 g L<sup>-1</sup> resulted in a notable drop of inactivation efficiency. The possible reason for such a reverse effect was the shielding effect of outer  $\text{VS}_4/\text{CP}$  particles with a higher  $\text{VS}_4/\text{CP}$  dosage [25]. Under this circumstance, irradiation of visible light would become the limiting factor, and inner  $\text{VS}_4/\text{CP}$  could not receive sufficient photons for photocatalytic disinfection [48]. Furthermore, various initial *E. coli* densities were investigated ( $10^6$  to  $10^9$  CFU mL<sup>-1</sup>, Fig. 5C), and an increased inactivation rate from 6.8 log, to 7.9 log, 8.9 log, and 9.7 log were achieved in 30 min, respectively. The results suggested an excellent disinfection performance of proposed  $\text{VS}_4/\text{CP}$ , especially under a higher bacteria density.

#### 3.4. Disinfection mechanism on a subcellular level

##### 3.4.1. Cell morphology

The TEM images of *E. coli* cell revealed an obvious cell-solution interface with an intact and smooth sphere shape (Fig. 6A). However, with the treatment of  $\text{VS}_4/\text{CP}$ , notable changes were observed with widened shape, rough membrane, and grain-like inner cell structure (Fig. 6B). It is worth noting that the majority of observed cells had comparable morphology, and hence only one cell was displayed for a demonstration purpose. The change in cell-solution interface could result from direct accumulation or adsorption of  $\text{VS}_4/\text{CP}$  on the cell

membrane. Changes of consistent inner cell structure to grain-like shape could be caused by penetration of  $\text{VS}_4/\text{CP}$  nanocomposite through cell membrane and clogging inside the cytoplasm. Hence, the TEM images indicated that, under visible light,  $\text{VS}_4/\text{CP}$  nanocomposite could alter the membrane structure of *E. coli* to facilitate direct penetration or physical accumulation, interrupting its normal metabolism. The results also suggested a potentially different subcellular mechanism than that of electrochemical disinfection, as no debris or disrupted cell was observed in the latter [16].

##### 3.4.2. TOC level and $\text{K}^+$ leakage

Cell membrane provides a perfect barrier between cell and the surrounding environment, and envelops the essential cytoplasm and organelles. When being exposed to the disinfectants, this barrier can be notably affected, leading to potential leakage of cytoplasm together with the organic substances and inorganic ions to the outside solution. Thus, the destruction extent of cell membrane and inactivation of *E. coli* cells can be indirectly revealed by quantification of TOC level and  $\text{K}^+$  concentration in the suspension. The TOC level in the suspension exhibited a dramatic drop from 28.2 mg L<sup>-1</sup> to 6.1 mg L<sup>-1</sup> (Fig. 7A), indicating a notable mineralization of *E. coli* cells under the  $\text{VS}_4/\text{CP}$  dosage of 0.1 g L<sup>-1</sup> [16]. The leakage of  $\text{K}^+$  from *E. coli* cells was profound throughout the test window (Fig. 7A), with an accelerated leakage rate as the experiment process continued. The  $\text{K}^+$  concentration in solution reached its peak value of 0.65 mg L<sup>-1</sup> at the end of experiment. The cellular  $\text{K}^+$  was essential to the well function of bacteria due to its vital role in maintaining a stable cell osmotic pressure, activation of intracellular enzymes, and most importantly balancing cytoplasm pH [49]. The leakage of  $\text{K}^+$  indicated a change in cell permeability and/or a disorder of cross-membrane  $\text{K}^+$  transport systems

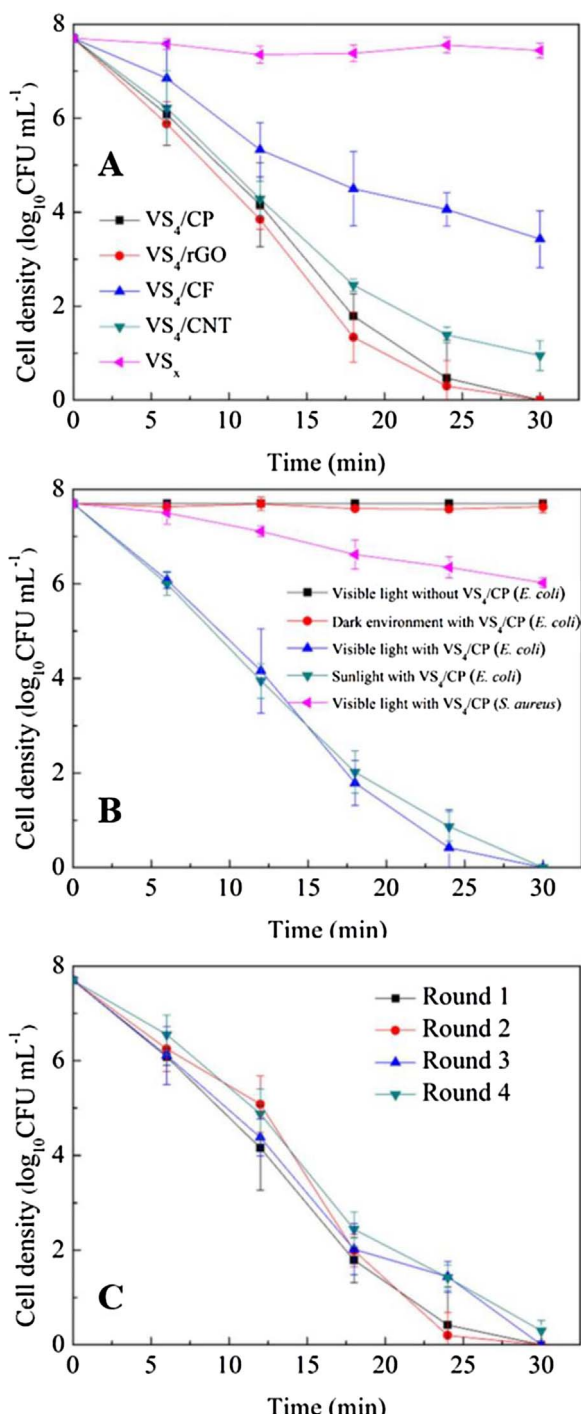


Fig. 4. Disinfection performance of (A) various carbon supported VS<sub>4</sub> nanocomposites, (B) VS<sub>4</sub>/CP under various light conditions, and (C) stability test of VS<sub>4</sub>/CP under simulated visible light and four successive applications.

and ion channels.

#### 3.4.3. Cell membrane property

Cell membrane property was evaluated with respect to membrane permeability quantified by penetration of extracellular substrate ONPG into cytoplasm and integrity by lipid peroxidation via measuring the peroxidation product malondialdehyde (MDA). Cell membrane permeability of ONPG was stable over the 30 min (0.09–0.17 μmol·min<sup>-1</sup> mg<sup>-1</sup> cell dry weight), suggesting no substantial physical damage (e.g. enlarged holes or cracks) during the disinfection process (Fig. 7B). Combining with the TEM image of the cell, it suggested that

**Table 1**  
Comparison of disinfection performance among several photocatalysts.

Photocatalyst	Time (h)	Cell Density (CFU mL <sup>-1</sup> )	Catalyst Dosage (g L <sup>-1</sup> )	Inactivation	Ref.
TiO <sub>2</sub> /Ag <sub>2</sub> O	1.0	10 <sup>3</sup>	1.00	3.0 log	[38]
Fe <sub>2</sub> O <sub>3</sub> -AgBr	4.0	10 <sup>7</sup>	0.05	7.0 log	[39]
GO/g-C <sub>3</sub> N <sub>4</sub>	2.0	10 <sup>7</sup>	0.10	7.0 log	[40]
GO-CdS	1.0	10 <sup>7</sup>	0.20	5.3 log	[41]
g-C <sub>3</sub> N <sub>4</sub> -AgBr	1.0	3.0 × 10 <sup>6</sup>	0.10	6.5 log	[42]
TiO <sub>2</sub> -rGO composites	3.0	10 <sup>6</sup>	0.02	5.3 log	[43]
VS <sub>4</sub> /CP nanocomposites	0.5	5.0 × 10 <sup>7</sup>	0.10	7.7 log	This study
		9.6 × 10 <sup>9</sup>	0.10	9.7 log	

VS<sub>4</sub>/CP might accumulate on or penetrate the membrane without damaging its physical structure. The unsaturated lipids on cell membrane could react with the generated active species to form MDA, and thus the MDA concentration is typically used as an indirect indicator for lipid peroxidation extent. The MDA concentration gradually increased over the disinfection time and ended up in 0.13 nmol mg<sup>-1</sup> cell dry weight (Fig. 7B), suggesting a minor change in membrane integrity [50]. According to the results, the VS<sub>4</sub>/CP nanocomposites might have affected the lipid portion of the cell membrane and mineralize the organic residuals, rendering enhanced leakage of K<sup>+</sup> and reduced membrane fluidity (less smooth in the TEM image) [51]. Further MP analysis revealed that a secondary peak located at relative fluorescence intensity 100 (RFI 100) was observed in the initial stage of reaction (Fig. 7C), which was one of the characteristic peaks for *E. coli* [28]. However, this peak position disappeared during the disinfection process (Fig. 7C), suggesting that the MP of *E. coli* went from a normal state to a collapsed state. The collapsed MP could lead to anomalous localization of the cell division related proteins, and thereby inhibit the reproduction of the bacterial cell, which was also considered as the major role in electrochemical disinfection systems [52].

#### 3.4.4. Intracellular substances

Directly penetration of VS<sub>4</sub>/CP nanocomposites into cytoplasm could seriously affect the intracellular components, leading to severe damage to the cell. The cellular ATP level gradually decreased with the disinfection progress, indicating a diminished cell metabolism rate as the disinfection process continued (Fig. 7D). ATP is the universal carrier of intracellular energy, and MP plays a crucial role in ATP synthesis [53]. The decreasing trend of cellular ATP level was similar to that of MP, indicating a general decline or even termination in the cell metabolism. The efficiencies of intracellular enzyme degradation gradually decreased (Fig. 7D), implying the gradually pronounced damage of the intracellular enzyme systems in the cytosol. As oxygen-containing radicals could hardly penetrate the cell membrane [28], this intracellular enzyme degradation could be caused by the direct entry of VS<sub>4</sub>/CP. The band on electrophoresis map gradually weakened over the disinfection progress (Fig. 7E), implying an accumulative DNA damage over the test window and notable DNA degradation as indicated by the fluorescence intensity. This result further illuminated the advantage of VS<sub>4</sub>/CP as a powerful disinfectant considering that some other disinfection approaches could hardly degrade DNA [28].

By evaluating a series of subcellular parameters across the disinfection window, it was revealed that membrane damage via lipid peroxidation, collapsed MP, and penetration-induced intracellular damage including DNA degradation and decreased ATP level were the main inactivation effects, resulting in serious damage of membrane structures and degradation of genetic materials in cytoplasm. These damages were highly effective, and the disinfection of *E. coli* by the VS<sub>4</sub>/CP nanocomposites was irreversible.

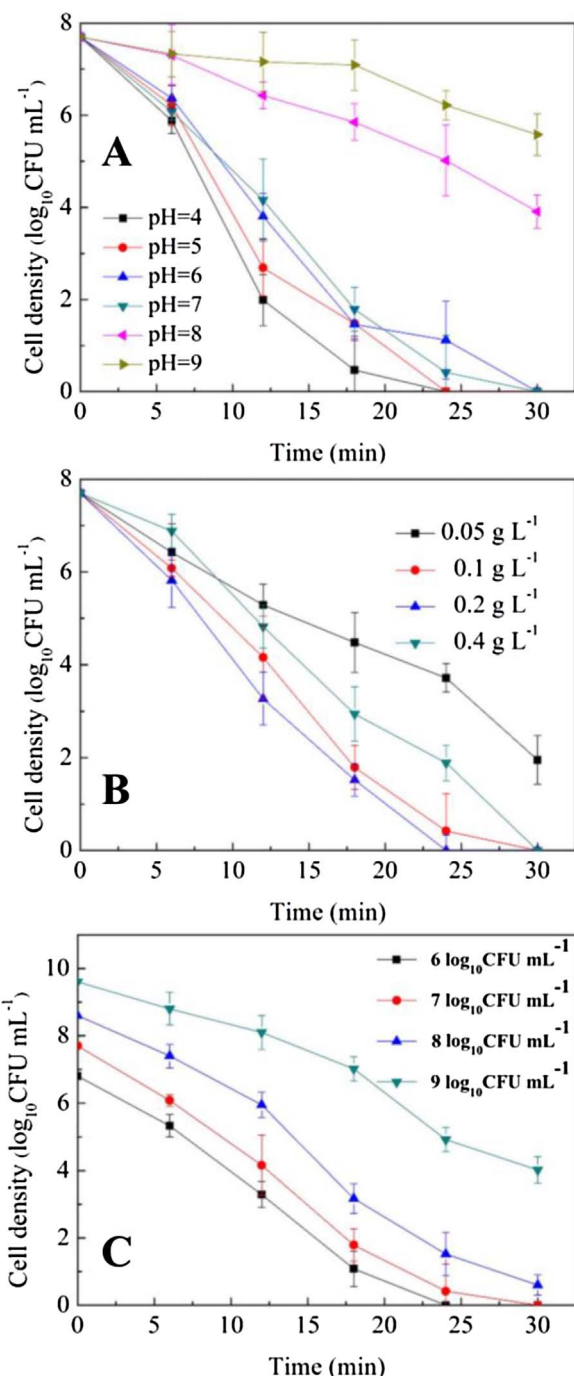


Fig. 5. Optimization of disinfection performance regarding (A) effect of solution pH with VS<sub>4</sub>/CP addition, (B) VS<sub>4</sub>/CP dosage, and (C) initial *E. coli* density. All experiments were performed under simulated visible light.

### 3.5. Disinfection mechanism on a photochemical level

A scavenger test was performed to understand the disinfection mechanism of the developed VS<sub>4</sub>/CP nanocomposites on a photochemical level. Photocatalytic disinfection via the VS<sub>4</sub>/CP nanocomposites is ascribed to the generation of active species, such as  $\cdot\text{OH}$ , H<sub>2</sub>O<sub>2</sub>,  $\cdot\text{O}_2^-$ , e $^-$ , and h $^+$  generated by through Eqs. (1)–(4) [46]. To further examine the mechanism of photocatalytic disinfection of *E. coli* cells by the VS<sub>4</sub>/CP nanocomposites, several scavenger compounds were added to the *E. coli* suspended solution to remove the corresponding active species, and the results were compared with that of the photocatalytic reaction without scavengers (Fig. 8). Addition of

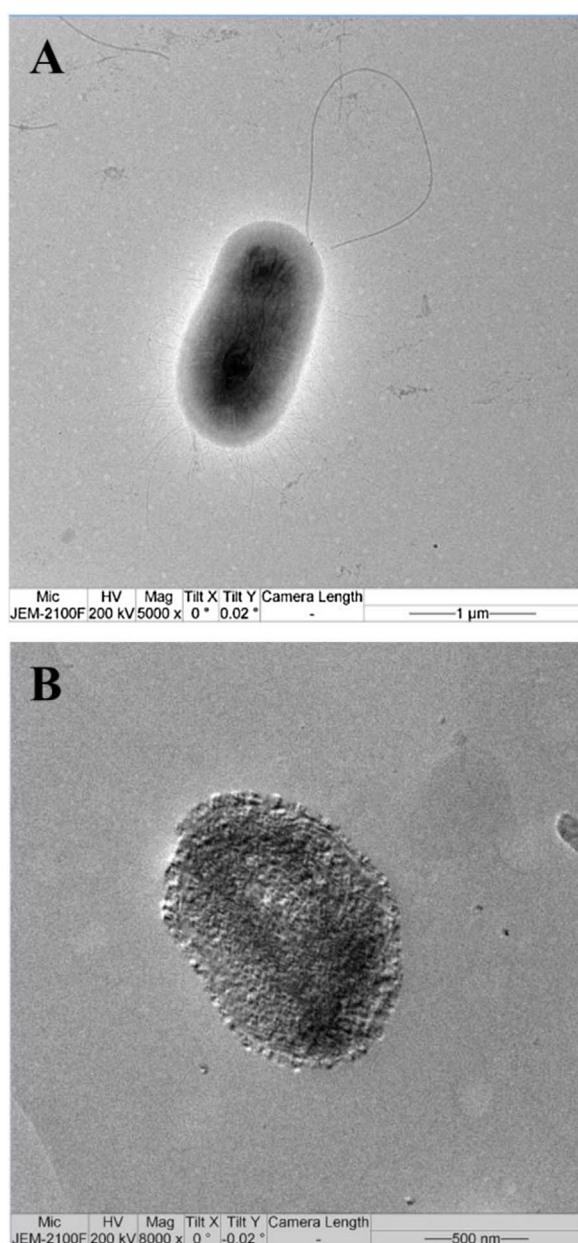


Fig. 6. TEM images of (A) pristine *E. coli* cell before adding VS<sub>4</sub>/CP, and (B) *E. coli* cell after VS<sub>4</sub>/CP dosage. Note that all observed cells were in uniform morphology so that one single cell could represent the majority of the population.

TEMPOL, sodium oxalate and Cr(VI) significantly inhibited the photo-disinfection by the VS<sub>4</sub>/CP nanocomposites with *E. coli* inactivation efficiency decreased to 7.7 log, 2.5 log, and 1.3 log, respectively, suggesting that  $\cdot\text{O}_2^-$ , h $^+$  and e $^-$  were crucial for successful photocatalytic disinfection of *E. coli* cells. Functions of  $\cdot\text{O}_2^-$  and e $^-$  were critical to this process with some auxiliary effects from h $^+$  because photocatalytic disinfection could happen through oxidation by active oxidants as well as reduction by electrons [54]. Similar observations were also obtained in other photocatalytic disinfection experiments with the main contribution from  $\cdot\text{O}_2^-$  and the complementary role of h $^+$  [46]. The addition of Fe(II)-EDTA and Isopropanol exhibited negligible influence on the overall disinfection performance (Fig. 8), with inactivation efficiencies of 7.7 log and inactivation of 1.1 log. It was worth noting that addition of scavenger compounds alone could not render any photo-disinfection effect (Fig. A3). Thus, the role of H<sub>2</sub>O<sub>2</sub> and  $\cdot\text{OH}$  in the photocatalytic disinfection via the VS<sub>4</sub>/CP nanocomposites could be minor [6].

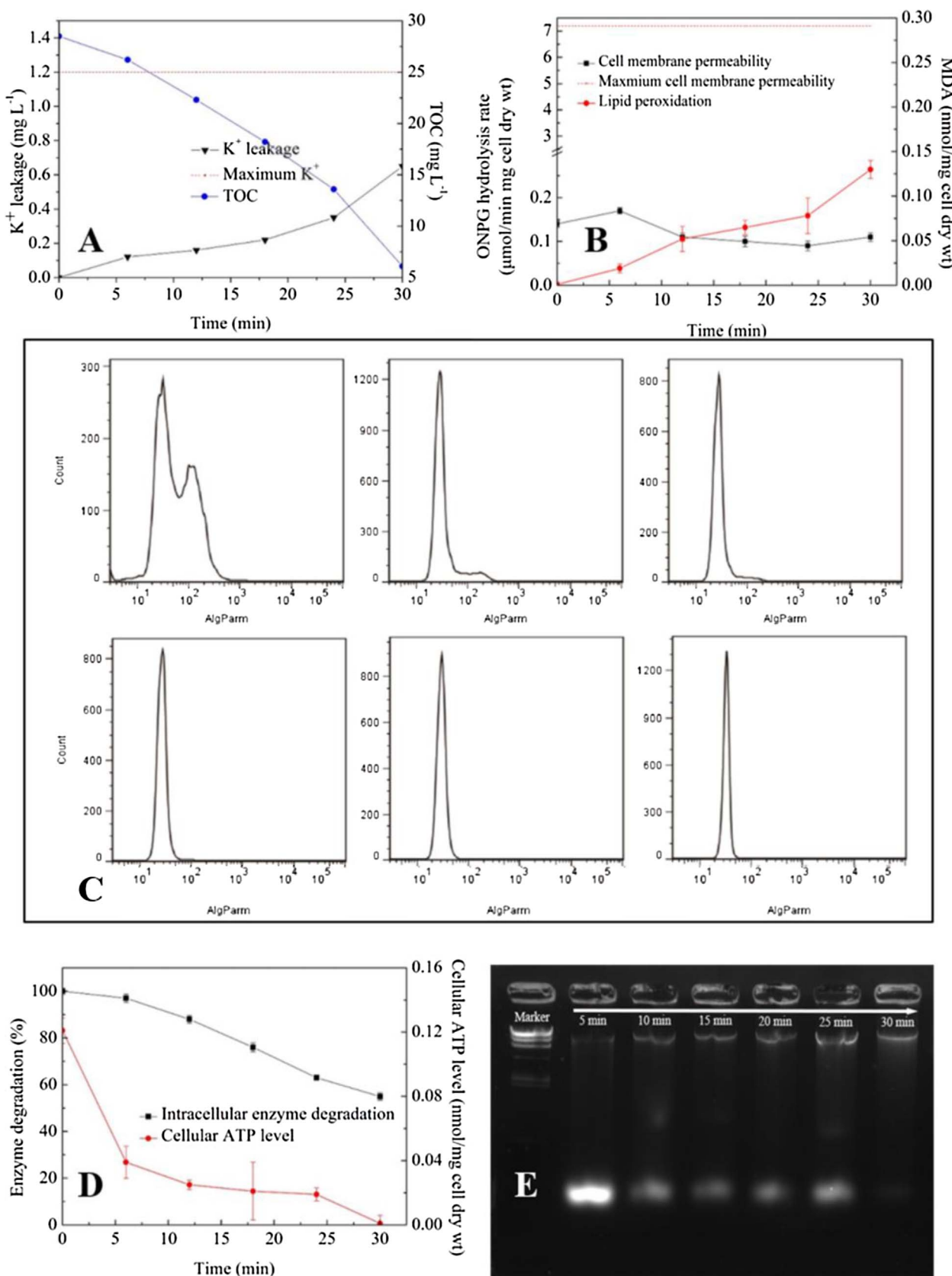
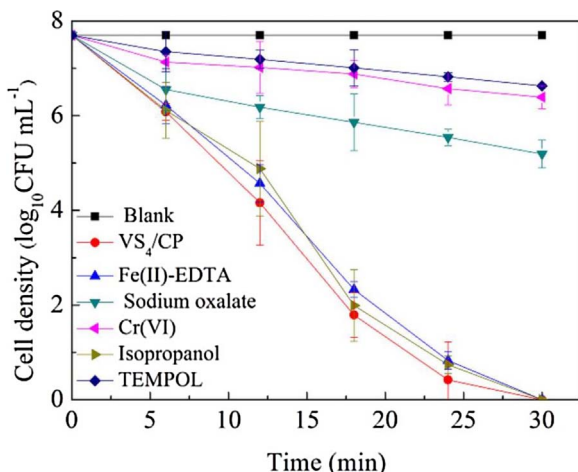


Fig. 7. Subcellular analysis of disinfection mechanism regarding (A) TOC level and  $K^+$  concentration in the suspension, (B) membrane permeability reflected by ONPG and lipid peroxidation reflected by MDA, (C) membrane potential, (D) cellular ATP level, and (E) electrophoresis map of extracted DNA. All experiments were performed in the default disinfection system (simulated visible light and catalyst dosage of 0.1 g L<sup>-1</sup>).



**Fig. 8.** Photochemical analysis of disinfection mechanism via addition of various scavenger compounds together with VS<sub>4</sub>/CP.

#### 4. Conclusions

In this study, a series of carbon supported Vanadium Tetrasulfide (VS<sub>4</sub>) nanocomposites were synthesized, and the lattice-structure VS<sub>4</sub>/CP exhibited excellent disinfection performance for removing *E. coli* (Gram-negative) under both simulated visible light and natural sunlight. The maximum inactivation rate was 9.7 log at 0.1 g L<sup>-1</sup> in 30 min, higher than those of the similar visible-light-driven nanomaterial disinfectants. A stable disinfection performance was obtained after multiple uses of VS<sub>4</sub>/CP materials or over a wide range of *E. coli* density. Subcellular characterization demonstrated that membrane damage (via mineralization, lipid peroxidation and collapsed membrane potential) and penetration-induced intracellular damage including DNA degradation and decreased ATP level could be the main inactivation principles. Photochemical investigation suggested that ·O<sub>2</sub><sup>-</sup>, h<sup>+</sup> and e<sup>-</sup> were crucial active species, and an acidic/neutral environment would favor the photocatalytic disinfection. Those results encourage further investigation and development of VS<sub>4</sub>/CP nanocomposites for water disinfection applications.

#### Acknowledgements

This research work was supported by the National Natural Science Foundation of China (NSFC, No. 91647115 and No. 41672237) and Beijing Nova Program (No. Z171100001117082). Shiqiang Zou was financially supported by a Fellowship from Water INTERface IGEP at Virginia Tech.

#### Appendix A. Supplementary data

Supplementary data associated with this article can be found, in the online version, at <http://dx.doi.org/10.1016/j.apcatb.2017.10.065>.

#### References

- [1] Q. Li, S. Mahendra, D.Y. Lyon, L. Brunet, M.V. Liga, D. Li, P.J. Alvarez, Antimicrobial nanomaterials for water disinfection and microbial control: potential applications and implications, *Water Res.* 42 (2008) 4591–4602.
- [2] F. Hossain, O.J. Perales-Perez, S. Hwang, F. Roman, Antimicrobial nanomaterials as water disinfectant: applications, limitations and future perspectives, *Sci. Total Environ.* 466 (2014) 1047–1059.
- [3] S.D. Richardson, M.J. Plewa, E.D. Wagner, R. Schoeny, D.M. DeMarini, Occurrence, genotoxicity, and carcinogenicity of regulated and emerging disinfection by-products in drinking water: a review and roadmap for research, *Mutat. Res. Rev. Mutat. Res.* 636 (2007) 178–242.
- [4] P. Fernández-Ibáñez, M. Polo-López, S. Malato, S. Wadhwa, J. Hamilton, P. Dunlop, R. D'sa, E. Magee, K. O'shea, D. Dionysiou, Solar photocatalytic disinfection of water using titanium dioxide graphene composites, *Chem. Eng. J.* 261 (2015) 36–44.
- [5] A. Ganguly, P. Trinh, K. Ramanujachary, T. Ahmad, A. Mugweru, A.K. Ganguli, Reverse micellar based synthesis of ultrafine MgO nanoparticles (8–10 nm): characterization and catalytic properties, *J. Colloid Interface Sci.* 353 (2011) 137–142.
- [6] R.P. Cavalcante, R.F. Dantas, B. Bayarri, O. González, J. Giménez, S. Esplugas, A. Machulek, Photocatalytic mechanism of metoprolol oxidation by photocatalysts TiO<sub>2</sub> and TiO<sub>2</sub> doped with 5% B: primary active species and intermediates, *Appl. Catal. B* 194 (2016) 111–122.
- [7] P. Louwakul, A. Saelo, S. Khemaaelakul, Efficacy of calcium oxide and calcium hydroxide nanoparticles on the elimination of *Enterococcus faecalis* in human root dentin, *Clin. Oral Investig.* (2016) 1–7.
- [8] H. Masoumbaigi, A. Rezaee, H. Hosseini, S. Hashemi, Water disinfection by zinc oxide nanoparticle prepared with solution combustion method, *Desalin. Water Treat.* 56 (2015) 2376–2381.
- [9] M. Załęska-Radziwiłł, N. Doskocz, DNA changes in *Pseudomonas putida* induced by aluminum oxide nanoparticles using RAPD analysis, *Desalin. Water Treat.* 57 (2016) 1573–1581.
- [10] E. Krieg, H. Weissman, E. Shirman, E. Shimoni, B. Rybchinski, A recyclable supramolecular membrane for size-selective separation of nanoparticles, *Nat. Nanotechnol.* 6 (2011) 141–146.
- [11] H.W. Liang, L. Wang, P.Y. Chen, H.T. Lin, L.F. Chen, D. He, S.H. Yu, Carbonaceous nanofiber membranes for selective filtration and separation of nanoparticles, *Adv. Mater.* 22 (2010) 4691–4695.
- [12] K.G. McGuigan, R.M. Conroy, H.-J. Mosler, M. du Preez, E. Ubomba-Jaswa, P. Fernandez-Ibáñez, Solar water disinfection (SODIS): a review from bench-top to roof-top, *J. Hazard. Mater.* 235 (2012) 29–46.
- [13] X. Chen, S.S. Mao, Titanium dioxide nanomaterials: synthesis, properties, modifications, and applications, *Chem. Rev.* 107 (2007) 2891–2959.
- [14] M.K. Seery, R. George, P. Floris, S.C. Pillai, Silver doped titanium dioxide nanomaterials for enhanced visible light photocatalysis, *J. Photochem. Photobiol. A Chem.* 189 (2007) 258–263.
- [15] L.K. Adams, D.Y. Lyon, P.J. Alvarez, Comparative eco-toxicity of nanoscale TiO<sub>2</sub>, SiO<sub>2</sub>, and ZnO water suspensions, *Water Res.* 40 (2006) 3527–3532.
- [16] Y. Long, J. Ni, Z. Wang, Subcellular mechanism of *Escherichia coli* inactivation during electrochemical disinfection with boron-doped diamond anode: a comparative study of three electrolytes, *Water Res.* 84 (2015) 198–206.
- [17] S. Pigeot-Rémy, F. Simonet, E. Errazuriz-Cerda, J. Lazzaroni, D. Atlan, C. Guillard, Photocatalysis and disinfection of water: identification of potential bacterial targets, *Appl. Catal. B* 104 (2011) 390–398.
- [18] M. Cho, J. Kim, J.Y. Kim, J. Yoon, J.-H. Kim, Mechanisms of *Escherichia coli* inactivation by several disinfectants, *Water Res.* 44 (2010) 3410–3418.
- [19] O.K. Dalrymple, E. Stefanakos, M.A. Trotz, D.Y. Goswami, A review of the mechanisms and modeling of photocatalytic disinfection, *Appl. Catal. B* 98 (2010) 27–38.
- [20] M. Berney, H.-U. Weilenmann, T. Egli, Flow-cytometric study of vital cellular functions in *Escherichia coli* during solar disinfection (SODIS), *Microbiology* 152 (2006) 1719–1729.
- [21] T.D. Cutler, J.J. Zimmerman, Ultraviolet irradiation and the mechanisms underlying its inactivation of infectious agents, *Anim. Health Res. Rev.* 12 (2011) 15–23.
- [22] R. Cai, B. Zhang, J. Shi, Z. He, Rapid photocatalytic decolorization of methyl orange under visible light using VS<sub>4</sub>/carbon powder nanocomposites, *ACS Sustain. Chem. Eng.* 5 (2017) 7690–7699.
- [23] G. Lui, G. Jiang, A. Duan, J. Broughton, J. Zhang, M.W. Fowler, A. Yu, Synthesis and characterization of template-free VS<sub>4</sub> nanostructured materials with potential application in photocatalysis, *Ind. Eng. Chem. Res.* 54 (2015) 2682–2689.
- [24] C.S. Rout, B.-H. Kim, X. Xu, J. Yang, H.Y. Jeong, D. Odokhuu, N. Park, J. Cho, H.S. Shin, Synthesis and characterization of patronite form of vanadium sulfide on graphitic layer, *J. Am. Chem. Soc.* 135 (2013) 8720–8725.
- [25] W. Guo, D. Wu, Facile synthesis of VS<sub>4</sub>/graphene nanocomposites and their visible-light-driven photocatalytic water splitting activities, *Int. J. Hydrogen Energy* 39 (2014) 16832–16840.
- [26] H. Irie, Y. Watanabe, K. Hashimoto, Carbon-doped anatase TiO<sub>2</sub> powders as a visible-light sensitive photocatalyst, *Chem. Lett.* 32 (2003) 772–773.
- [27] T. Tachikawa, S. Tojo, K. Kawai, M. Endo, M. Fujitsuka, T. Ohno, K. Nishijima, Z. Miyamoto, T. Majima, Photocatalytic oxidation reactivity of holes in the sulfur- and carbon-doped TiO<sub>2</sub> powders studied by time-resolved diffuse reflectance spectroscopy, *J. Phys. Chem. B* 108 (2004) 19299–19306.
- [28] F. Dong, S. Guo, H. Wang, X. Li, Z. Wu, Enhancement of the visible light photocatalytic activity of C-doped TiO<sub>2</sub> nanomaterials prepared by a green synthetic approach, *J. Phys. Chem. C* 115 (2011) 13285–13292.
- [29] D. Chen, Z. Jiang, J. Geng, Q. Wang, D. Yang, Carbon and nitrogen co-doped TiO<sub>2</sub> with enhanced visible-light photocatalytic activity, *Ind. Eng. Chem. Res.* 46 (2007) 2741–2746.
- [30] B. Hu, X. Zhao, H. Liu, Z. Liu, T. Song, Y. Wang, L. Tang, X. Xia, G. Tang, D. Ji, Quantification of the impact of aerosol on broadband solar radiation in North China, *Sci. Rep.* 7 (2017).
- [31] C. Liu, D. Kong, P.-C. Hsu, H. Yuan, H.-W. Lee, Y. Liu, H. Wang, S. Wang, K. Yan, D. Lin, Rapid water disinfection using vertically aligned MoS<sub>2</sub> nanofilms and visible light, *Nat. Nanotechnol.* 11 (2016) 1098–1104.
- [32] S. Zou, S. Yao, J. Ni, High-efficient nitrogen removal by coupling enriched autotrophic-nitrification and aerobic-denitrification consortiums at cold temperature, *Bioresour. Technol.* 161 (2014) 288–296.
- [33] S. Yao, J. Ni, Q. Chen, A.G.L. Borthwick, Enrichment and characterization of a bacteria consortium capable of heterotrophic nitrification and aerobic denitrification at low temperature, *Bioresour. Technol.* 127 (2013) 151–157.
- [34] W. Wang, L. Zhang, T. An, G. Li, H.-Y. Yip, P.-K. Wong, Comparative study of

visible-light-driven photocatalytic mechanisms of dye decolorization and bacterial disinfection by B–Ni-codoped TiO<sub>2</sub> microspheres: the role of different reactive species, *Appl. Catal. B* 108 (2011) 108–116.

[35] X. Xu, Z. Gao, Z. Cui, Y. Liang, Z. Li, S. Zhu, X. Yang, J. Ma, Synthesis of Cu<sub>2</sub>O octadecahedron/TiO<sub>2</sub> quantum dot heterojunctions with high visible light photocatalytic activity and high stability, *ACS Appl. Mater. Interfaces* 8 (2015) 91–101.

[36] C. Karunakaran, G. Abiramasundari, P. Gomathisankar, G. Manikandan, V. Anandi, Cu-doped TiO<sub>2</sub> nanoparticles for photocatalytic disinfection of bacteria under visible light, *J. Colloid Interface Sci.* 352 (2010) 68–74.

[37] K.G. McGuigan, R.M. Conroy, H.-J. Mosler, M. d. Preez, E. Ubomba-Jaswa, P. Fernandez-Ibañez, Solar water disinfection (SODIS): a review from bench-top to roof-top, *J. Hazard. Mater.* 235–236 (2012) 29–46.

[38] B. Liu, L. Mu, B. Han, J. Zhang, H. Shi, Fabrication of TiO<sub>2</sub>/Ag<sub>2</sub>O heterostructure with enhanced photocatalytic and antibacterial activities under visible light irradiation, *Appl. Surf. Sci.* 396 (2017) 1596–1603.

[39] T.W. Ng, L. Zhang, J. Liu, G. Huang, W. Wang, P.K. Wong, Visible-light-driven photocatalytic inactivation of *Escherichia coli* by magnetic Fe<sub>2</sub>O<sub>3</sub>–AgBr, *Water Res.* 90 (2016) 111–118.

[40] L. Sun, T. Du, C. Hu, J. Chen, J. Lu, Z. Lu, H. Han, Antibacterial activity of graphene oxide/g-C<sub>3</sub>N<sub>4</sub> composite through photocatalytic disinfection under visible light, *ACS Sustain. Chem. Eng.* 5 (2017) 8693–8701.

[41] C.-H. Deng, J.-L. Gong, G.-M. Zeng, Y. Jiang, C. Zhang, H.-Y. Liu, S.-Y. Huan, Graphene–CdS nanocomposite inactivation performance toward *Escherichia coli* in the presence of humic acid under visible light irradiation, *Chem. Eng. J.* 284 (2016) 41–53.

[42] J. Deng, J. Liang, M. Li, M. Tong, Enhanced visible-light-driven photocatalytic bacteria disinfection by gC<sub>3</sub>N<sub>4</sub>-AgBr, *Colloids Surf. B. Biointerfaces* 152 (2017) 49–57.

[43] B.R. Cruz-Ortiz, J.W. Hamilton, C. Pablos, L. Díaz-Jiménez, D.A. Cortés-Hernández, P.K. Sharma, M. Castro-Alfárez, P. Fernández-Ibañez, P.S. Dunlop, J.A. Byrne, Mechanism of photocatalytic disinfection using titania-graphene composites under UV and visible irradiation, *Chem. Eng. J.* 316 (2017) 179–186.

[44] H.M. Yadav, S.V. Otari, R.A. Bohara, S.S. Mali, S.H. Pawar, S.D. Delekar, Synthesis and visible light photocatalytic antibacterial activity of nickel-doped TiO<sub>2</sub> nanoparticles against Gram-positive and Gram-negative bacteria, *J. Photochem. Photobiol. A. Chem.* 294 (2014) 130–136.

[45] A.-G. Rincon, C. Pulgarin, Effect of pH, inorganic ions, organic matter and H<sub>2</sub>O<sub>2</sub> on *E. coli* K12 photocatalytic inactivation by TiO<sub>2</sub>: implications in solar water disinfection, *Appl. Catal. B* 51 (2004) 283–302.

[46] J. Liang, C. Shan, X. Zhang, M. Tong, Bactericidal mechanism of BiOI–AgI under visible light irradiation, *Chem. Eng. J.* 279 (2015) 277–285.

[47] S. Zou, Z. He, Enhancing wastewater reuse by forward osmosis with self-diluted commercial fertilizers as draw solutes, *Water Res.* 99 (2016) 235–243.

[48] M.-Y. Alikhani, S.-M. Lee, J.-K. Yang, M. Shirzad-Siboni, H. Peeri-Dogaheh, M.-S. Khorasani, M.-A. Nooshak, M.-R. Samarghandi, Photocatalytic removal of *Escherichia coli* from aquatic solutions using synthesized ZnO nanoparticles: a kinetic study, *Water Sci. Technol.* 67 (2012) 557–563.

[49] M.V. Radchenko, K. Tanaka, R. Waditee, S. Oshimi, Y. Matsuzaki, M. Fukuhara, H. Kobayashi, T. Takabe, T. Nakamura, Potassium/proton antiport system of *Escherichia coli*, *J. Biol. Chem.* 281 (2006) 19822–19829.

[50] H. Selcuk, Disinfection and formation of disinfection by-products in a photoelectrocatalytic system, *Water Res.* 44 (2010) 3966–3972.

[51] R. Hong, T.Y. Kang, C.A. Michels, N. Gadura, Membrane lipid peroxidation in copper alloy-mediated contact killing of *Escherichia coli*, *Appl. Environ. Microbiol.* 78 (2012) 1776–1784.

[52] H. Li, X. Zhu, J. Ni, Inactivation of *Escherichia coli* in Na<sub>2</sub>SO<sub>4</sub> electrolyte using boron-doped diamond anode, *Electrochim. Acta* 56 (2010) 448–453.

[53] P. Dimroth, G. Kaim, U. Matthey, Crucial role of the membrane potential for ATP synthesis by F(1)F(o) ATP synthases, *J. Exp. Biol.* 203 (2000) 51–59.

[54] S. Ning, H. Lin, Y. Tong, X. Zhang, Q. Lin, Y. Zhang, J. Long, X. Wang, Dual couples Bi metal depositing and Ag@AgI islanding on BiOI 3D architectures for synergistic bactericidal mechanism of *E. coli* under visible light, *Appl. Catal. B* 204 (2017) 1–10.